

Organic & Biomolecular Chemistry

Accepted Manuscript



This is an *Accepted Manuscript*, which has been through the Royal Society of Chemistry peer review process and has been accepted for publication.

Accepted Manuscripts are published online shortly after acceptance, before technical editing, formatting and proof reading. Using this free service, authors can make their results available to the community, in citable form, before we publish the edited article. We will replace this *Accepted Manuscript* with the edited and formatted *Advance Article* as soon as it is available.

You can find more information about *Accepted Manuscripts* in the [Information for Authors](#).

Please note that technical editing may introduce minor changes to the text and/or graphics, which may alter content. The journal's standard [Terms & Conditions](#) and the [Ethical guidelines](#) still apply. In no event shall the Royal Society of Chemistry be held responsible for any errors or omissions in this *Accepted Manuscript* or any consequences arising from the use of any information it contains.

Targeting DNA with small molecules: a comparative study of a library of azonia aromatic chromophores

Cite this: DOI: 10.1039/x0xx00000x

Rosa M. Suárez,^{a‡} Pedro Bosch,^{a‡} David Sucunza,^{a*} Ana M. Cuadro,^a Alberto Domingo,^b Francisco Mendicuti^c and Juan J. Vaquero^{a*}

Received 00th January 2012,
Accepted 00th January 2012

DOI: 10.1039/x0xx00000x

www.rsc.org/

A library of azonia aromatic cations has been studied in order to gain an insight into the role of the size, shape and charge distribution on the fluorescence, DNA interactions and DNA sequence selectivity properties. Fluorescence-based thermal denaturation experiments, spectrofluorimetric titrations, circular dichroism measurements and theoretical simulations have shown that some of the studied chromophores have interesting fluorescence properties and two of them also show a consistent DNA-binding ability by intercalation, with a potential preference for AT-rich sequences.

Introduction

Coralyne is probably the most widely studied quinolizinium-based alkaloid. Interest in this compound is due to several significant properties associated with its structure, a penta-substituted dibenzo[*a,g*]quinolizinium system.¹ In addition to the most commonly studied properties of this alkaloid, such as cytotoxicity,² intercalative DNA binding³ and potent topoisomerase inhibition,⁴ other remarkable properties have been reported, e.g., applications as fluorescent probes,⁵ reagents for the photoinduction of DNA damage,⁶ RNA binding,⁷ human telomeric quadruplex DNA,⁸ and hemoglobin.⁹ Complex formation between coralayne and *c*-di-AMP¹⁰ and α -, β -, and γ -cyclodextrin¹¹ has also been reported.

The interest in this alkaloid has led to a significant amount of research concerned with the synthesis and study of coralayne analogues and other related azonia cations that contain a quinolizinium system as the core heterocycle, with recent significant contributions by Ihmels and col.,¹² Becq and col.,¹³ *inter alia* (Figure 1).

It has been shown that fused polyaromatic azonia cations are a representative family of DNA intercalators with fluorescence properties.³ The binding of these molecules to DNA is characterized by the insertion of planar aromatic rings between the DNA base pairs through π -stacking interactions. The positive charge enhances the propensity of these molecules to bind to DNA due to attractive ionic interactions between the cation and the phosphate backbone.¹⁴

A number of polyaromatic azonia cations are fluorescent due to the presence of a scaffold that is related to cyanine dyes,¹⁵ a synthetic dye family with a general polymethine structure that has been widely applied in various areas associated with non-linear optics, photochromism, light energy transformation and so on.¹⁶ For this reason, some condensed polyaromatic azonia cations have been used as fluorescent probes.^{12b}

Our recent contributions in the field of azonia heterocycles have focused on the development of general synthetic procedures by ring-closing metathesis reactions (RCM) of azinium aza-dienes,¹⁷ new methods for the functionalization of the quinolizinium cation by palladium-promoted reactions,¹⁸ and the investigation of quinolizinium as an acceptor unit in non-linear optical (NLO) and two photon absorption (2PA) cationic chromophores.¹⁹ The synthesis of some aza-quinolizinium-type cations and their potential as DNA intercalators and antiproliferative compounds has also been reported from our laboratory.²⁰

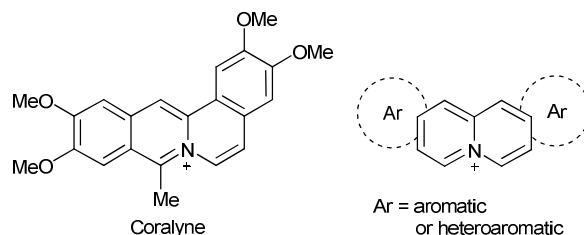


Figure 1. Structure of coralayne and general structure of quinolizinium-based azonia cations.

We report here our results from a comparative study in which a library of azonia cations has been investigated in order to gain an insight into the influence that the size, shape and charge distribution has on some of their properties, with potential applications as dyes and DNA probes. The fluorescence, DNA interactions and DNA sequence selectivity were compared.

Results and discussion

With the aim of covering different possibilities of size, shape and charge distribution of the chromophores, a library of twelve

aromatic azonia cations based on different heterocyclic cores was studied. Compounds **1–4** (Figure 2) are based on the quinolizinium system fused with benzo-, dibenzo-, naphtho- and indolo- moieties. Three examples (**5–7**) are based on an aza-quinolizinium core and another five cations (**8–12**) share an azoloquinolinium unit as the cationic moiety.

The role of size was studied by comparing the properties of compounds such as **8–11** or **1** and **2(3)**. Compounds **2** and **3** are appropriate to obtain data related to charge distribution within the chromophore. In the cases of **4** and **5** the presence of an additional nitrogen in the latter compound should provide information about the effect of replacing a methylene group next to the quaternary nitrogen atom of quinolizinium with another nitrogen.³ On the basis of previous studies, the results of which seem to support a better DNA binding profile for non-linear chromophores,²¹ compounds such as **4**, **6**, **7** and **12** were compared to assess the role of shape. These latter compounds are all tetracyclic but they have different ring arrangements.

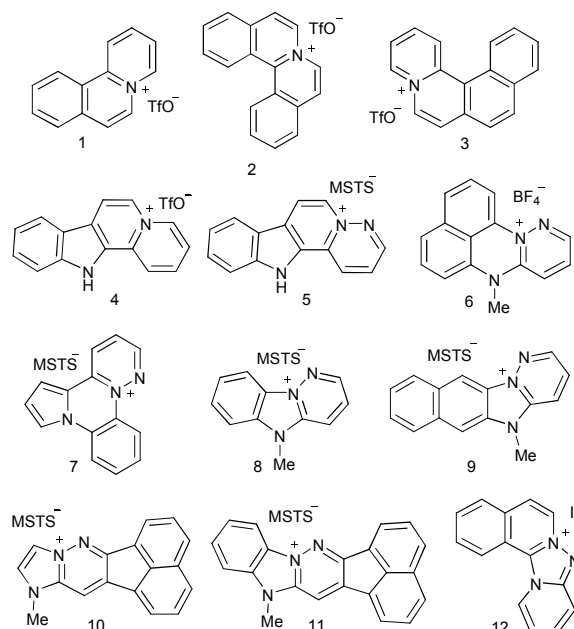
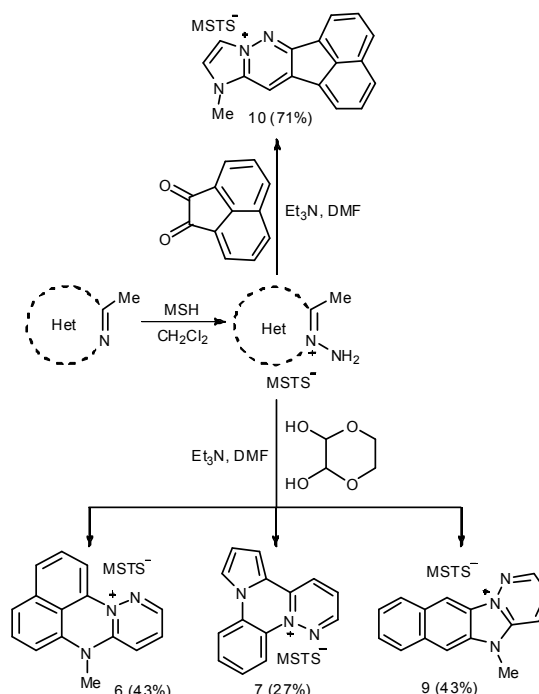


Figure 2. Structure of the twelve selected azonia cations.

Eight of the aforementioned salts were synthesized in our laboratory either by a ring-closing metathesis (RCM) reaction or by a Westphal condensation as key steps. Thus, quinolizinium-based derivatives **1**, **2**, **3** and **4** were obtained by the first strategy,¹⁷ azaquinoliziniums **5** and **8** by Westphal condensation with [1,4]-dioxane-2,3-diol (DODO)²² and **11** by condensation of the corresponding *N*-amino imidazolium salt with acenaphthenequinone.²³ Finally, triazoloisoquinolinium derivative **12** was obtained by iodination of the isoquinolinium *N*-(2'-pyridyl)aminide.²⁴

Compounds **6**, **7**, **9** and **10** were previously unknown and they were all prepared by condensation of DODO or acenaphthenequinone with the corresponding *N*-aminoazolinium or azolinium salts. Thus, *N*-amination of 1,2-dimethyl-1*H*-perimidine,²⁵ 4-methylpyrrolo[1,2-*a*]quinoxaline²⁶ and 1,2-dimethyl-1*H*-naphtho[2,3-*d*]imidazole²⁷ with *O*-mesitylenesulfonylhydroxylamine (MSH)²⁸ gave the corresponding salts, which were subsequently treated with DODO in the presence of triethylamine to afford **6**, **7** or **9** in overall yields of 27–43% (Scheme 1). The corresponding salt obtained from commercially available 1,2-dimethylimidazole was reacted with acenaphthenequinone to afford **10** in good yield (71%).



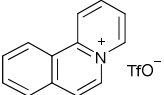
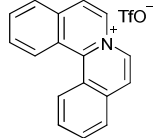
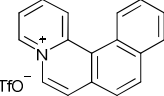
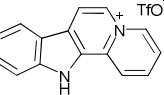
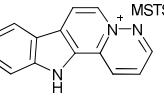
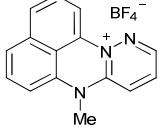
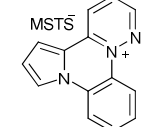
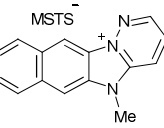
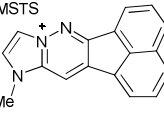
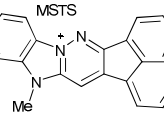
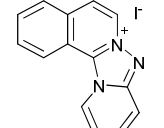
Scheme 1. Synthesis of derivatives **6**, **7**, **9** and **10**.

In order to identify the azonia structures that are most interesting as potential dyes and DNA probes, the DNA-binding capacity was tested and the photophysical properties for the **1–12** chromophoric derivatives were studied. DNA binding studies were carried out by FRET-based thermal denaturation using custom synthetic oligonucleotides with defined AT- or GC-rich sequences. The absorption and emission spectra were monitored (Figures 2S and 3S of the Supporting Information). In most cases the emission spectra of the derivatives, upon excitation of the maximum for the low energy absorption peak (λ_{max}), have a single band. The former low energy bands in the absorption spectra are usually attributed to the π - π^* charge transfer transition, which is characteristic for high conjugated systems. The λ_{max} location is rather sensitive to the degree of conjugation and the electron-donating/withdrawing characteristic of the substituents at the quinolizinium, aza-quinolizinium or azoloquinolinium cores. The results of DNA-binding assays and the photophysical parameters for **1–12** derivatives, as well as molar absorptivities, fluorescence quantum yields and fluorescence lifetimes are given in Table 1. The fluorescence quantum yields in methanol show rather different values and the fluorescence intensity profiles fit monoexponential or biexponential decay functions depending on the nature of the system.

The DNA-binding assays revealed that compounds **4**, **10** and **11** have a high affinity for this biomolecule, whereas **2**, **3**, **5** and **6** have a low affinity and **1**, **7**, **8**, **9** and **12** do not have any affinity for DNA. More interestingly, all of the compounds that had good DNA-binding properties showed a weak interaction with GC-rich oligonucleotides but a detectable and rapid increase in T_m from lower ligand concentrations in the case of AT-rich oligonucleotides.

Several general conclusions can be drawn from the data discussed above. As one would expect, DNA binding is closely related to the size of the molecule. Pentacyclic and hexacyclic compounds show good DNA-binding properties, whereas the tricyclic compounds do not have affinity for DNA. A clear trend was not observed for tetracycles as some compounds had high affinity for DNA but others had none. These data are consistent with results obtained previously by our group, which showed that a minimum

Table 1. DNA-binding affinities and base sequence selectivities. Some photophysical parameters: molar absorptivities (ϵ , $M^{-1}cm^{-1}$) at the wavelength used for excitation in the steady-state measurements (λ_{max} , nm), maximum of the emission wavelength (λ_{em} , nm), fluorescence quantum yields (ϕ_f), using a quinine solution in 0.1 M sulfuric acid as standard,²⁹ and fluorescence lifetimes (τ or $\langle\tau\rangle$, ns) monitored at the excitation/emission wavelengths of 335 nm/ λ_{em} for ligands **1–12** in methanol at 25 °C. (*) Weighted average lifetimes by using eq. 1, for those compounds whose fluorescence intensity profiles were fitted to biexponential decay functions.

	Structure	DNA binding	Relative GC/AT preference	ϵ (λ_{max})	λ_{em}	ϕ_f	τ_{ex} ($\langle\tau\rangle$), ns
1		No	---	3180 (338)	361	0.23	3.6
2		Low	AT	10430 (371)	400	0.35	5.9
3		Low	AT	8240 (369)	419	0.15	5.0
4		Yes	AT	5600 (334)	467	0.15	11.8*
5		Low	AT	11480 (331)	424	0.03	13.9
6		Very low	No	9400 (325)	435	< 0.01	4.7*
7		No	---	14700 (354)	472	0.02	5.3*
8		No	---	7210 (312)	442	0.33	16.7
9		No	---	12100 (351)	437	< 0.01	3.6*
10		Yes	AT	13453 (360)	427	0.41	7.45
11		Yes	AT	11850 (387)	450	0.25	4.4
12		No	---	7380 (320)	353	0.18	6.3

number of four fused rings are needed to produce an interaction with DNA in these systems.^{23a} However, it is unclear whether, in this series, there is a clear correlation between the shape and charge distribution of the molecule and its DNA binding activity. As for the photophysical properties, quinolinizinium and imidazolium moieties generally give rise to higher fluorescence quantum yields, although the value for derivative **9** is surprisingly low.

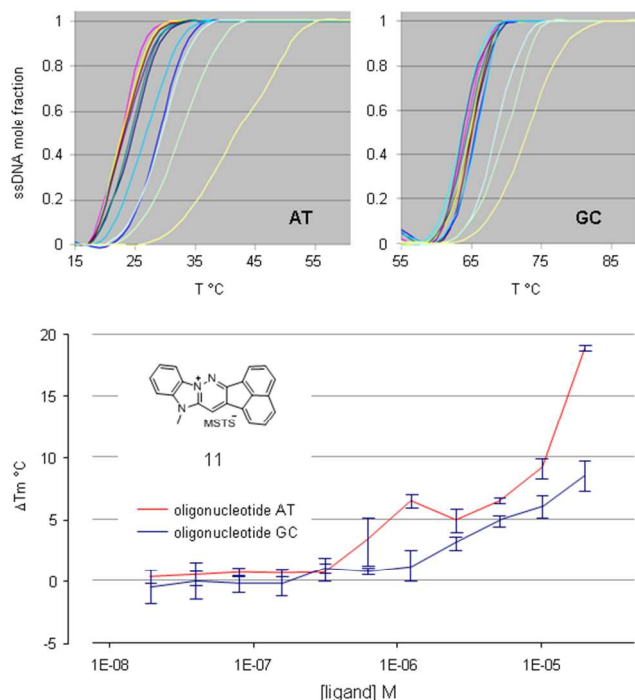


Figure 3. Melting curves (upper panels) and plot of the experimental ΔT_m versus ligand concentration on the logarithmic scale (lower panel) obtained for reaction mixtures of compound **11** and double-stranded DNA oligonucleotides of different base compositions and sequences. Oligonucleotide AT (red line). -5'-CAATTAATATAAC-3' and its complementary. Oligonucleotide GC (blue line). -5'-GCGCGGCGTCCGGGCC-3' and its complementary. Each data point is the average of two separate experiments. Ligand concentrations (M): 1.95 E-08, 3.91 E-08, 7.81 E-08, 1.56 E-07, 3.13 E-07, 6.25 E-07, 1.25 E-06, 2.5 E-06, 5.0 E-06, 1.0 E-05 and 2.0 E-05.

Of the twelve selected structures, derivatives **4**, **10** and **11** show the highest affinity for DNA, with **4**^{17a} and **11** (Figure 3) suggesting a possible preference for AT-rich sequences. For this reason, these compounds were chosen for a detailed study with DNA. Nevertheless, in order to prove the validity of the methods and conclusions, compound **8**, one of the fluorescent compounds that did not show affinity for DNA, was also studied.

Binding of ligands **4**, **8** and **11** with ctDNA

The emission spectra obtained at 25 °C for **4**, **8** and **11** in PBS buffer solutions (pH = 7.4) during titrations are shown in Figure 4. Excitation wavelengths were fixed at 334, 310 and 387 nm for **4**, **8** and **11**, respectively. The emission spectra in the absence or in the presence of calf-thymus DNA (ctDNA) also exhibited similar features to those obtained in methanol, i.e., a single band centred around 470, 460 and 460 nm, respectively. These bands were not displaced significantly upon ctDNA addition. However, rather different changes in the fluorescence intensity were observed. Quenching of the fluorescence intensity was observed on increasing [DNA] for **4** and **11**, whereas for **8** the fluorescence intensity

remained virtually unchanged. These observations indicate a binding interaction for **4** and **11** with DNA that does not seem to take place for **8**. The normalized variation of the fluorescence intensity of these ligands is shown in Figure 5 (left), ($I_0 - I$)/ I_0 (I measured as the area under the emission spectra and subscript zero denoting the absence of ctDNA) against [DNA].

The variation of the fluorescence anisotropy (r), obtained by equation 2 (Supporting Information), versus [DNA] at 25 °C is shown in Figure 5 (right). The r values and signs for solutions of **4**, **8** and **11** in the absence of ctDNA denote different orientations of the absorption and emission transition moments, buffer sizes and rotational diffusion in the low viscosity buffer solvent. The changes in r observed upon addition of aliquots of ctDNA were different depending on the type of ligand. The r values for **4** and **11** increased significantly with [DNA]. An increase is barely observed for **8**. This trend for increasing r is typical of the formation of a ligand:DNA complex whose rotational relaxation time is higher when compared to that of the free ligand.

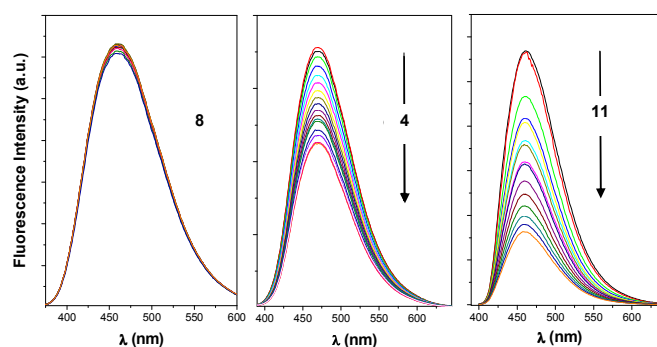


Figure 4. Emission spectra for solutions of ligands **8**, **4** and **11** ($[L] = 1.9, 1.9$ and 1.94×10^{-5} mol/L, respectively) and upon the addition of DNA aliquots during the titration at 25 °C.

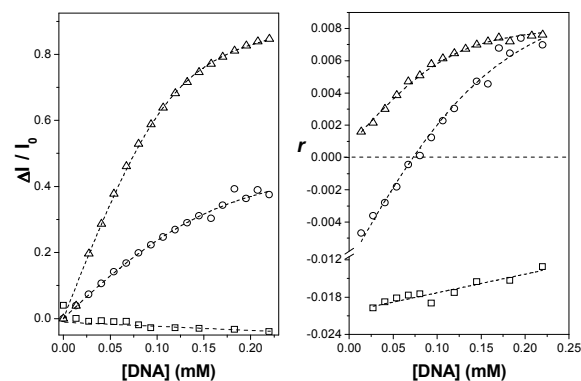


Figure 5. (left) Normalized variation of the fluorescence intensity for buffer solutions (PBS buffer solutions containing 5% of DMSO) of ligands **8**, **4** and **11** ($[dye] = 1.9, 1.9$ and 1.94×10^{-5} mol/L respectively, at these concentrations any complex precipitation was observed during titrations) at 25 °C versus [DNA]. (Right) Fluorescence anisotropy versus [DNA] for the same solutions at 25 °C. Symbols correspond to **4** (○), **8** (□) and **11** (△). r values were monitored at the maximum of emission upon excitation at 334, 310 and 387 nm, respectively.

The curves depicted in Figure 5 (left) for **4** and **11** were obtained by adjusting the experimental data to equation 10 (Supporting Information) and these show a good fit. The curves provide values for the binding constants of ca. $(2.8 \pm 1.3) \times 10^4$

and $(6.9 \pm 2.6) \times 10^4 \text{ M}^{-1}$ for **4** and **11**, respectively. These values are of the same order of magnitude as those for some previously reported naphtho- and indolo-annulated quinolizinium DNA ligands.³ The average number of nucleic base pairs per bound ligand was 8.0 ± 0.4 and 5.9 ± 0.3 , respectively. However, compound **8** does not seem to interact with DNA. The curves depicted in Figure 5 (right) for the anisotropy changes for **4** and **11** were obtained by fitting the experimental data to an equation similar to **9** (Supporting Information), but using r instead of the fluorescence intensity, I , and the K and n values obtained from fluorescence intensity measurements.

Fluorescence intensity decay profiles for ligands **4**, **8** and **11** did not seem to be particularly sensitive to the presence of ctDNA. The lifetimes, which are collected in Table 2, were quite similar for all ligand solutions in the absence or in the presence of ctDNA. However, whereas decay profiles for **8** and **11** were fitted to a monoexponential decay function, profiles for **4** were fitted to a bi-exponential function with lifetime components of ~ 4.5 ns and ~ 15 ns. Nevertheless, $\langle \tau \rangle$ barely changed upon addition of DNA. These facts could be attributed to a rapid photoinduced electron transfer reaction where DNA bases and ligand are involved. This would likely decrease DNA-bound ligand lifetimes to values shorter than even the nanosecond detection apparatus limit.^{3,30}

Table 2. Lifetime components, contributions and weighted averages for the dye intercalator aqueous solutions in the absence and in the presence of ctDNA (in parenthesis) at 25 °C. The [DNA] was the highest [DNA] used in previous experiments. Excitation wavelength with a NanoLed emitting at 335 nm.

	λ_{em} (nm)	τ_1 (ns)	%	τ_2 (ns)	%	$\langle \tau \rangle$ (ns)
4	465	4.3 (4.5)	54.2 (39.6)	14.8 (15.0)	45.8 (60.4)	9.1 (10.9)
8	442	4.1 (4.2)	100	---	---	---
11	460	4.3 (4.3)	100	---	---	---

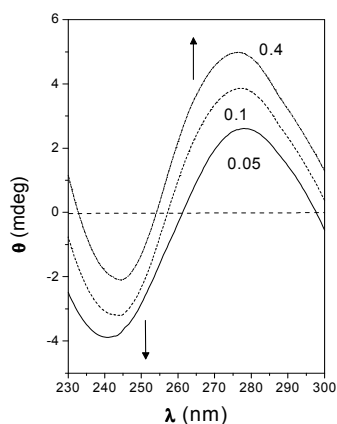


Figure 6. CD spectra (as ellipticity, θ) in the region of DNA absorption at 25 °C for buffer solutions (PBS buffer solutions containing 5% of DMSO) of ligand **11** in the presence of ctDNA ($[\text{DNA}] = 3.57 \times 10^{-4} \text{ M}$) at several ligand/DNA molar ratios.

The interaction of compounds **4**, **8** and **11** with DNA was also studied by circular dichroism (CD) spectroscopy. The CD spectrum in the region of the DNA absorption can provide information about changes in its secondary structure caused by ligand-DNA interactions.³¹ As depicted in Figure 6 for **11**, the ctDNA shows the

typical DNA B-form CD spectrum with positive and negative Cotton effects centered at ~ 278 and ~ 245 nm, which are due to base stacking and right-handed polynucleotide helicity, respectively. Changes in the two bands are quite sensitive to the mode of interaction with small molecules.³² While groove binding of small molecules with DNA shows little or no perturbation on the base stacking and helicity bands, intercalation usually enhances the intensities of both bands. As depicted in Figure 6, the intensities of both bands increase significantly upon increasing the concentration of **11**, thus indicating intercalative binding to DNA. These changes in the DNA CD spectra are a consequence of the increase in base pair-ligand interactions and also some unwinding and lengthening of the DNA helix upon dye intercalation. Similar changes were observed for **4**.

In contrast to the above, achiral compounds like **4**, **8** and **11** do not have CD activity. However, a CD signal can be induced (ICD) as a consequence of a possible non-degenerate coupling of their transition moments and the average dipole moments of the nucleic bases. Consequently, the observation of a CD spectrum in the absorption region of the ligand is irrefutable evidence for the existence of ligand-DNA interaction. The intensity and the sign of the ICD depend on the position and the orientation of the chromophore relative to the DNA bases. An intercalator exhibits a weak negative ICD when the transition moment for the corresponding absorption band is oriented along the pseudolong axis of the binding DNA pocket (parallel to the bisector of the base pairs). However, a strong positive ICD is expected when the transition moment is polarized perpendicular to the long axis of the binding pocket. The ICD signal for a groove-bound ligand is usually one or two orders of magnitude larger than that for an intercalated one. In addition, if the transition moment is oriented along the groove that forms a 45° angle with the bases, the ICD is expected to be positive.^{3,12c,32a,33}

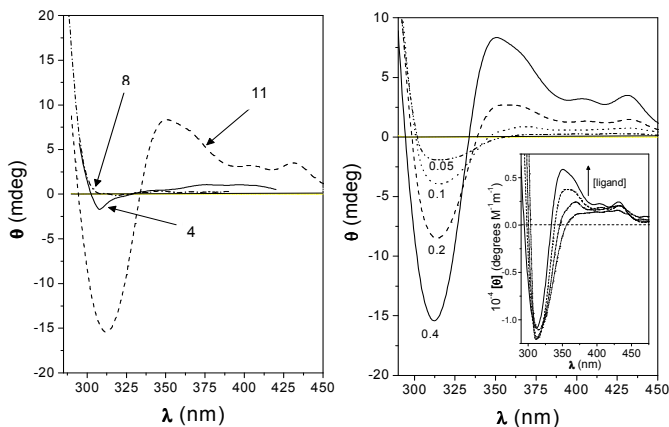


Figure 7. CD spectra, as ellipticity, θ in mdegrees for (left) **4**, **8** and **11** ligand buffer solutions in the presence of ctDNA at $[\text{DNA}] = 3.57 \times 10^{-4} \text{ M}$ at a $[\text{ligand}]/[\text{DNA}] = 0.4$; (right) **11** at several ligand/DNA molar ratios at 25 °C. The CD spectra, as molar ellipticity, is superimposed.

The CD spectra for intercalators **4**, **8** and **11** in the presence of DNA at a fixed ligand:DNA molar ratio of 0.4 are shown in Figure 7 (left). ICD was not observed for **8** at any of the molar ratios (0.05, 0.1, 0.2 or 0.4) as interactions did not take place. However, the CD spectra for **4** and **11**, at all of the ratios used, exhibited two regions with negative and positive Cotton effects that extend in the ~ 295 – 335 nm and 335 – 460 nm ranges, respectively (Figure 7, right). Nevertheless, the CD signals were much weaker for **4** than **11**. These asymmetric negative and positive induced bands seem to match

other bands that appear in the absorption spectra of the compounds. Thus, the presence of exciton coupling due to the aggregation of **4** and **11**, which associate with the DNA, could be discounted.^{3,12c,33b}

In addition, the molar ellipticity $[\theta]$ shows an increase in the positive band with $[\text{ligand}]$ that did not occur for the negative band. In analogy with other quinolinizinium derivatives, and on the assumption that the transition moments of the bands that appear at longer wavelengths ($\sim 335\text{--}400\text{ nm}$) are almost parallel to the long ligand axis, the sign of the bands reveals intercalation of **4** and **11** with their long-molecular axis perpendicular to the DNA binding pocket.^{3,12c} Consequently, the negative $\sim 295\text{--}335\text{ nm}$ band is consistent with an absorption band whose transition moment is oriented along the short molecular axis. The relatively low quantitative ellipticity values, which are positive, especially for **4**, also discard the presence of groove binding.

Molecular Mechanics and Molecular Dynamics simulations

The total binding energy values are shown in Figure 8 along with van der Waals and electrostatics contributions as a function of the oo' distance along the y coordinate, for the most favourable orientation of **11** approaching the DNA by the major or minor groove sides. Two different approaches were considered: (i) parallel to the planar bases as an intercalator (Figure 8, left panel) or (ii) parallel to the pair of helices as a groove binder (Figure 8, right panel). Intercalation takes place with hardly any potential energy barriers. However, as one would expect, in the groove-binding approach, when guest **11** is oriented at 45° with respect the pair of bases, high potential barriers are observed at $y = \pm 5\text{ \AA}$ due to the repulsive van der Waals ligand interaction with DNA base pairs. The results show that electrostatic interactions are mostly responsible for the stabilization of the system. It is worth noting that for the minimum binding structures (MBE) of **11** the intercalator ligand is oriented in such a manner that its main axis is oriented parallel to the TA and AT central bases pocket axis but is slightly outside it on the major groove side (1 in Figure 8). However, the main long axis of **11** is almost parallel to both DNA chains in 2. The arrows in Figure 8 indicate the ligand acenaphthene group.

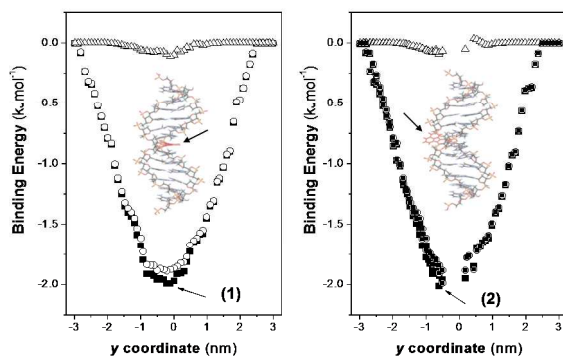


Figure 8. Total binding energies (■), van der Waals (△) and electrostatic (○) contributions as a function of the oo' distance (nm) measured along the y coordinate for the ligand **11** approaching DNA as an intercalator (left) and as a groove binder (right). Superimposed are the MBE structures, designated as 1 and 2, viewed from the positive x axis (note the location of the ligand). (1) and (2) MBE structures were used as starting conformations for the MD simulations.

The histories of the **11**-DNA binding energies and contributions and oo' distances obtained from analysis of the 1.0 ns MD trajectories at 300 K in the water-solvated (1) MBE structure are

shown in Figure 9 (upper panel). The results indicate that **11**-DNA interactions are favourable for intercalation throughout the whole trajectory. As with MM, the most important contributions to stabilization were the electrostatics. The van der Waals interactions contributed 10% of the total binding energy (Figure 9, upper panel). The history for the y coordinate of the centre of ligand **11** (o') is depicted in Figure 9 (bottom panel). The intercalator tends to move inside the bases pocket close to the y coordinate value of -1 (\AA) . This movement also involves rotation and a subsequent increase in the angle between the bisector of the bases pocket and the long axis of the ligand in such a way that, after $\sim 0.7\text{ ns}$ and at the end of the trajectory, it is oriented almost perpendicular to the pocket and with the acenaphthene group lying slightly outside it by the minor groove face (see Figure 10). The latter structure is consistent with the sign of the bands observed in the ICD spectrum for the region in which **11** absorbs (Figure 7, right). In addition, the average of the angle between the AT and TA base pair planes and the plane of intercalator **11** throughout the trajectory is close to zero, as one would expect.

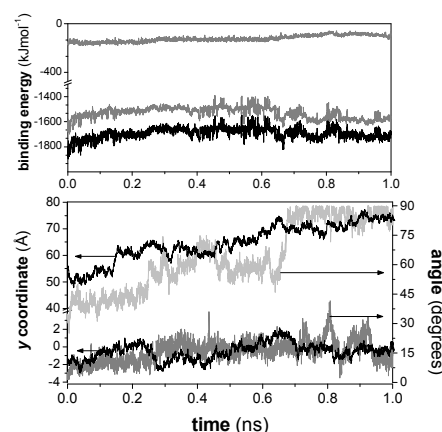


Figure 9. (upper panel) Histories for binding energies (black) and electrostatics (grey) and van der Waals (light grey) contributions obtained from the analysis of the 1 ns MD trajectory at 300 K starting from the minimized MBE structure (1). (bottom panel) Idem for the y coordinate (bottom black line) of the centre of the **11** molecule (o'), the end-to-end DNA helix distance (upper black line), the averaged angle between the plane of both AT and TA pairs of bases and the plane of **11** (dark grey) and the angle between the bisector of pocket bases and the long axis of **11** (light grey).

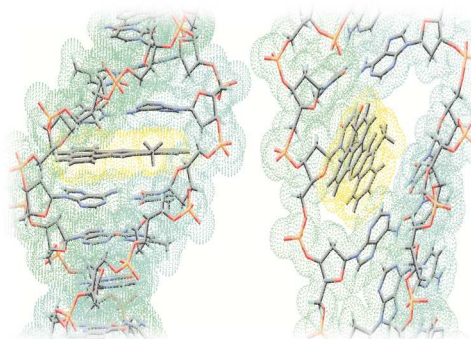


Figure 10. Snapshots of the 1 ns MD trajectory at 300 K showing the location of the ligand. Structures correspond to the central portion of the **11**-DNA complex: (left) at time = 0 ns, i.e., starting minimized MBE structure (1); (right) at time = 0.8 ns from the beginning of the trajectory.

Another characteristic observation after intercalation is that a monotonic increase of the end-to-end DNA distance (Figure 9) occurs with time. This change is due to the slight unwinding and elongation of the DNA helix upon intercalation. This helix enlargement and the base-ligand interactions are also consistent with the increase in the intensity of the bands observed in the CD spectrum at the DNA region upon **11**-DNA complexation (Figure 7, left). Details of some snapshots of the complex structures at different times are shown in Figure 10. At 0.8 ns **11** is oriented as one would expect from the ICD spectrum.

When MD is performed starting from (2), i.e., the MBE structure for the groove approach, the most important feature is that during the first steps of the trajectory the ligand penetrates and prefers to intercalate between the two AT-TA base pairs. Whereas the plane of the molecule of **11** is also almost parallel to the plane of both pairs of bases (average plane angle of $13\pm 7^\circ$), in this case the angle between the long axis and the binding pocket is around 45° and, at the end of the trajectory, this decreases to around 30° (average angle of $39\pm 10^\circ$), which is not consistent with the experimental evidence.

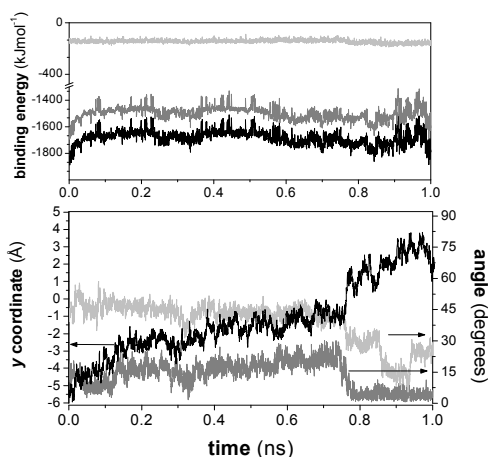


Figure 11. (upper panel) Histories for binding energies (black) and electrostatics (grey) and van der Waals (light grey) contributions obtained from the analysis of the 1 ns MD trajectory at 300 K starting from the minimized MBE **11**-DNA groove binding structure, namely (2), obtained from MM calculations. (bottom panel) Idem for the y coordinate (bottom black line) for the centre of the dye molecule (σ), the averaged angle between the plane of both AT and TA pairs of bases and the plane of the **11** molecule (dark grey) and the angle between the bisector of pocket bases and the long **11** axis (light grey).

A similar situation occurred for DNA complexation by ligand **4**. As shown in Figure 4S of the Supporting Information, intercalation of compound **4** is also favourable and electrostatic interactions are mainly responsible for this stabilization. For the MBE structure the results indicate that **4** is mainly parallel to both central pairs of bases when it intercalates DNA, but that it prefers to locate slightly outside the pocket by the minor groove face. Analysis of the MD trajectories also showed that interactions for the intercalation are favourable throughout the whole trajectory, with electrostatics being the most important contributions to the stabilization (Figure 5S, Supporting Information). In this case, the centre of intercalator **4** tends to stay around the $y = +1$ (Å) coordinate. The average of the angle between the bisector of the bases pocket and the long axis of the dye is $62.1\pm 9.8^\circ$, which means that it deviates slightly from 90° . This behaviour is responsible for the weakness of the ICD signal. In addition, the angle between the AT and TA base pair planes and the plane of intercalator **4** is close to zero, as one

would expect. As in the previous study, a monotonic increase in the end-to-end DNA distance occurs with time. A portion of the MBE structure for the **4**-DNA complex used as the starting conformation for the 1 ns MD trajectory at 300 K (left) and those obtained from the analysis of the MD trajectory (right) are represented in Figure 6S (Supporting Information).

Conclusions

Fluorescence, DNA interactions and DNA sequence selectivity properties of twelve different azonia cations have been studied. Among them, tetracyclic indoloquinolinium **4** and hexacyclic benzimidazolium **11** present the highest affinity for DNA, with a potential preference for AT-rich sequences. Photophysical and DNA binding experiments showed that both compounds are fluorescent and they bind to double-stranded DNA by intercalation. The findings described here will allow further studies on **4** and **11** or its derivatives as DNA probes.

Experimental

Synthetic procedures

General information

Reagents were purchased at the highest commercial quality available and were used without further purification, unless stated otherwise. Reactions were monitored by thin-layer chromatography (TLC) carried out on 0.25 mm E. Merck silica gel plates (60FS-254) with visualization by UV light. Column chromatography was performed using silica gel (60 F254, 70–200 mm) as the stationary phase. All melting points were determined in open capillary tubes on a Stuart Scientific SMP3 melting point apparatus and are uncorrected. IR spectra were obtained on a Perkin-Elmer FTIR spectrum 2000 spectrophotometer. ^1H and ^{13}C NMR spectra were recorded with either Varian Gemini (200 MHz), Varian Mercury VX-300, Varian Unity 300 or 500 MHz spectrometer at room temperature. Chemical shifts are given in ppm (d) downfield from TMS. Coupling constants (J) are in Hertz (Hz) and signals are described as follows: s, singlet; d, doublet; t, triplet; br, broad; m, multiplet; ap, apparent. High-resolution analysis (TOF) was performed on an Agilent 6210 time-of-flight LC/MS. 1,2-Dimethyl-1*H*-perimidine,²⁵ 4-methylpyrrolo[1,2-*a*]quinoxaline,²⁶ 1,2-dimethyl-1*H*-naphtho[2,3-*d*]imidazole,²⁷ *O*-mesitylenesulfonyl-hydroxylamine (MSH),²⁸ and [1,4]-dioxane-2,3-diol (DODO)²² were prepared according to procedures described in the literature.

7-Methyl-7*H*-pyridazino[1,6-*a*]perimidin-12-ium tetrafluoroborate (**6**)

A solution of MSH (108 mg, 0.5 mmol) in anhydrous CH_2Cl_2 (3 mL) was added to a solution of 1,2-dimethyl-1*H*-perimidine (75 mg, 0.38 mmol) in CH_2Cl_2 (3 mL). The mixture was stirred for 15 h at room temperature. The resulting *N*-amine salt was isolated by filtration and washed with Et_2O and petroleum ether. A mixture of this *N*-amine salt (110 mg, 0.27 mmol), DODO (32 mg, 0.27 mmol) and triethylamine (37 μL , 0.27 mmol) in anhydrous DMF (3 mL) was heated at 70°C for 2 h. The dark red solid residue was filtered off and treated with HBF_4 (1.2 equiv., 48% w/w water) at room temperature for 7 h. The crude product was purified by alumina column chromatography (gradient from CH_2Cl_2 to 1:9 MeOH/ CH_2Cl_2) to give compound **6** as a dark red powder (53 mg, 0.17 mmol, 43%). M.p.: $199\text{--}205^\circ\text{C}$. IR (KBr) $\nu_{\text{cm}^{-1}}$: 765, 1179, 1489, 1583, 1640, 2358, 3059, 3432. ^1H -NMR (200 MHz, CD_3OD) δ (ppm): 3.73 (s, 3H), 7.21 (dd, $J = 7$ Hz, $J = 1$ Hz, 1H), 7.54–7.68 (m, 3H), 7.83 (d, $J = 8$ Hz, 1H), 8.00–8.39 (m, 2H), 8.37 (dd, $J = 10$ Hz,

$J = 1$ Hz, 1H), 8.84 (dd, $J = 4$ Hz, $J = 1$ Hz, 1H). ^{13}C -NMR (50 MHz, CD_3OD) δ (ppm): 35.5, 109.6, 111.9, 121.6, 124.1, 126.2, 128.1, 129.3, 129.6, 134.5, 135.1, 135.9, 146.0, 151.1. MS (ESI): $[\text{M}^+]$ 234.1; HRMS m/z calculated for $\text{C}_{15}\text{H}_{12}\text{N}_3$ $[\text{M}^+]$: 234.1026. Found 234.1032. Anal. Calcd for $\text{C}_{15}\text{H}_{12}\text{BF}_4\text{N}_3$: C, 56.11; H, 3.77; N, 13.09. Found: C, 55.94; H, 3.92; N, 13.29.

Pyridazino[1,6-*a*]pyrrolo[2,1-*c*]quinoxalin-13-ium mesitylenesulfonate (7)

A solution of MSH (88 mg, 0.41 mmol) in anhydrous CH_2Cl_2 (3 mL) was added to a solution of 4-methylpyrrolo[1,2-*a*]quinoxaline (62 mg, 0.34 mmol) in CH_2Cl_2 (3 mL). The mixture was stirred for 5 h at room temperature. The resulting *N*-amine salt was isolated by filtration and washed with Et_2O and petroleum ether. A mixture of this *N*-amine salt (100 mg, 0.25 mmol), DODO (30 mg, 0.25 mmol) and triethylamine (35 μL , 0.25 mmol) in EtOH (4 mL) was heated at 76 °C for 4.5 h. The reaction mixture was concentrated under reduced pressure until dryness and triturated with acetone. The solid was filtered off and washed with acetone and petroleum ether to give compound 7 as a dark green powder (39 mg, 0.09 mmol, 27%). M.p: 135–138 °C. IR (KBr) ν cm^{-1} : 680, 1189, 1451, 1624, 3466. ^1H -NMR (300 MHz DMSO- d_6) δ (ppm): 2.15 (s, 3H), 2.47 (s, 6H), 6.72 (s, 2H), 7.35 (dd, $J = 2.6$ Hz, $J = 4.2$ Hz, 1H), 7.81 (tap, $J = 8.4$ Hz, $J = 8.7$ Hz, 1H), 8.02 (tap, $J = 8.4$ Hz, $J = 8.7$ Hz, 1H), 8.25 (dd, 4.2 Hz, $J = 1.2$ Hz, 1H), 8.38 (dd, $J = 9$ Hz, $J = 4.7$ Hz, 1H), 8.64 (d, 8.7 Hz, 1H), 8.85 (d, $J = 8.7$ Hz, 1H), 9.03 (d, $J = 1.6$ Hz, 1H), 9.31 (dd, $J = 9.0$ Hz, $J = 1.6$ Hz 1H), 9.38 (dd, $J = 4.7$ Hz, $J = 1.6$ Hz, 1H). ^{13}C -NMR (75 MHz DMSO- d_6) δ (ppm): 19.8, 22.3, 115.8, 116.3, 117.1, 119.7, 120.5, 122.6, 126.8, 127.2, 129.4, 130.4, 132.0, 132.1, 135.4, 135.7, 139.4, 142.4, 146.1, 148.9. MS (ESI): $[\text{M}^+]$ 220.1; HRMS m/z calculated for $\text{C}_{14}\text{H}_{10}\text{N}_3$ $[\text{M}^+]$: 220.0869. Found 220.0859. Anal. Calcd for $\text{C}_{23}\text{H}_{21}\text{N}_3\text{O}_3\text{S}$: C, 65.85; H, 5.05; N, 10.02. Found: C, 65.66; H, 5.12; N, 9.91.

5-Methyl-5*H*-naphtho[2',3':4,5]imidazo[1,2-*b*]pyridazin-12-ium mesitylenesulfonate (9)

A solution of MSH (174 mg, 0.81 mmol) in anhydrous CH_2Cl_2 (2 mL) was added to a solution of 1,2-dimethyl-1*H*-naphtho[2,3-*d*]imidazole (106 mg, 0.54 mmol) in CH_2Cl_2 (2 mL). The mixture was stirred for 1 h at room temperature. The resulting *N*-amine salt was isolated by filtration and washed with Et_2O and petroleum ether. A mixture of the *N*-amine salt (206 mg, 0.50 mmol), DODO (60 mg, 0.50 mmol) and triethylamine (70 μL , 0.50 mmol) in anhydrous DMF (3 mL) was heated at 70 °C for 1 h. The reaction mixture was concentrated under reduced pressure until dryness and triturated with Et_2O . The solid was filtered off and washed with acetone to give compound 9 as a yellow powder (99.7 mg, 0.23 mmol, 43%). M.p: 233–235 °C (decomposition). IR (KBr) ν cm^{-1} : 677, 1015, 1085, 1191, 1522, 1622, 2365, 3045. ^1H -NMR (300 MHz, MeOD) δ (ppm): 2.05 (s, 3H), 2.41 (s, 6H), 4.20 (s, 3H), 6.75 (s, 2H), 7.61–7.70 (m, 2H), 8.15–8.26 (m, 3H), 8.55 (s, 1H), 8.74 (d, $J = 8.2$ Hz, 1H), 8.99 (s, 1H), 9.07 (d, $J = 4.6$ Hz, 1H). ^{13}C -NMR (75 MHz, MeOD) δ (ppm): 20.8, 23.2, 31.3, 110.9, 112.9, 121.4, 128.0, 128.8, 129.1, 129.4, 130.0, 131.6, 131.9, 132.2, 132.5, 135.3, 138.1, 140.0, 140.8, 144.5, 147.3. MS (ESI): $[\text{M}^+]$ 234.1; HRMS m/z calculated for $\text{C}_{15}\text{H}_{12}\text{N}_3$ $[\text{M}^+]$: 234.1026. Found 234.1027. Anal. Calcd for $\text{C}_{24}\text{H}_{23}\text{N}_3\text{O}_3\text{S}$: C, 66.49; H, 5.35; N, 9.69. Found: C, 66.70; H, 5.20; N, 9.56.

11-Methyl-11*H*-acenaphtho[1,2-*e*]imidazo[1,2-*b*]pyridazin-8-ium mesitylenesulfonate (10)

A solution of MSH (0.61 g, 2.83 mmol) in anhydrous CH_2Cl_2 (3 mL) was added to a solution of commercially available 1,2-dimethylimidazole (0.18 g, 1.89 mmol) in CH_2Cl_2 (3 mL). The

mixture was stirred for 1 h at room temperature. The resulting *N*-amine salt was isolated by filtration and washed with Et_2O and petroleum ether. A mixture of the *N*-amine salt (0.49 g, 1.59 mmol), acenaphthoquinone (0.29 g, 1.59 mmol) and sodium acetate (0.13 g, 1.59 mmol) in ethanol (12 mL) was heated under reflux for 5 h. The reaction mixture was concentrated under reduced pressure until dryness and triturated with water. The solid was filtered off and washed with water and acetone to give compound 10 as a pale brown solid (0.61 g, 1.33 mmol, 71%). M.p: 260–261 °C. IR (KBr) ν cm^{-1} : 678, 1017, 1086, 1191, 1220, 1532, 3028, 3126, 3448. ^1H -NMR (300 MHz, DMSO- d_6) δ (ppm): 2.12 (s, 3H), 2.47 (s, 6H), 4.41 (s, 3H), 6.69 (s, 2H), 7.98 (tap, $J = 7.6$ Hz, 2H), 8.31–8.47 (m, 1H), 8.85 (d, $J = 2.1$ Hz, 1H), 9.37 (s, 1H). ^{13}C -NMR (50 MHz, DMSO- d_6) δ (ppm): 19.8, 22.2, 33.9, 111.0, 117.9, 122.6, 123.6, 126.2, 128.1, 128.8, 128.9, 129.2, 129.6, 130.4, 134.0, 134.9, 135.0, 135.2, 135.5, 142.3, 156.1. MS (ESI $^+$) m/z : 258.1. Anal. Calcd for $\text{C}_{26}\text{H}_{23}\text{N}_3\text{O}_3\text{S}$: C, 68.25; H, 5.07; N, 9.18. Found: C, 67.96; H, 5.11; N, 9.36.

Photophysical properties

Absorption spectra were recorded on a UV-Vis Uvikon 941 (Kontron Instruments) spectrophotometer. Steady-state fluorescence measurements were carried out by using a PTI Quanta Master spectrofluorimeter equipped with a Xenon flash lamp as a light source, with single concave grating monochromators and Glan–Thompson polarizers in the excitation and emission paths. Detection was carried out with a photomultiplier cooled by a Peltier system. Slit widths were selected at 6 nm for both excitation and emission paths and polarizers were fixed at the ‘magic angle’ conditions. Fluorescence decay measurements were performed on a time-correlated single-photon-counting FL900 Edinburgh Instruments Spectrometer. A monochromatic NanoLed (Horiba) emitting at 335 nm was used as the excitation source. Double concave grating monochromators were employed at both excitation and emission paths. Photons were detected by a red-sensitive cooled (by a Peltier system) photomultiplier. The data acquisition was carried out by using 1024 channels of a multichannel analyser with a time window width of 200 ns. A total of 10,000 counts in the maximum peak channel were taken for each measurement. The instrumental response function was regularly achieved by measuring the scattering of a Ludox solution. Intensity fluorescence profiles were fitted to multi-exponential decay functions by using the iterative deconvolution method.³⁴ The equations used are given in the Supporting Information.

Theoretical protocols for Molecular Mechanics and Molecular Dynamics calculations

Molecular Mechanics (MM) and Molecular Dynamics (MD) calculations were performed to study the forces responsible for the binding of quinolinizinium dyes to DNA and to assess the stability of the system. Calculations were performed with Sybyl X-2.0³⁵ and the Tripos Force Field.³⁶ B-DNA helical fragments, whose charges were derived using the Gasteiger and Marsili method, contained twelve nucleotides with a CGCGAATTCGCG sequence (approximately the percentage of the ctDNA bases). Charges for ligands were obtained by using the Gaussian suite of quantum chemical programs at the HF/6-31G(d) level of theory.³⁷ A relative permittivity $\epsilon = 1$ was used for electrostatic contributions in the presence of explicit water ($\epsilon = 3.5$ for some preliminary calculations in vacuum). Water solvation was performed using the Molecular Silverware (MS) algorithm and periodic boundary conditions (PBC).³⁸ Non-bonded cut-off distances for MM and for MD

were set at 12 Å. Optimizations were carried out using the simplex algorithm and the conjugate gradient was used as a termination method, with gradients of 3.0 Kcal/molÅ for the calculations carried out in water.³⁹ For further information and figures, see Supporting Information.

DNA binding experiments

1. DNA calf thymus binding

Concentrated solutions of ligands **4**, **8** and **11** in DMSO (Aldrich, HPLC grade) were diluted with a phosphate buffered saline solution (PBS) at pH = 7.4 containing 5% DMSO to give concentrations of 1.90×10^{-5} , 1.90×10^{-5} and 1.94×10^{-5} mol/L, respectively. Calf thymus DNA (high molecular weight sodium salt, ctDNA) was purchased from Aldrich and dissolved in Milli-Q water to obtain a ~2 mg/mL solution. The ctDNA concentration (per base pair) of this solution, determined by UV-Vis using $\epsilon(260 \text{ nm}) = 13,200 \text{ M}^{-1}\text{cm}^{-1}$, was 4.1×10^{-3} mol/L.⁴⁰ For titrations, 10 µL aliquots of this ctDNA solution were added to the 10 mm quartz cell containing 3 mL of the above ligand solutions and the samples were stirred prior to measurement to ensure temperature equilibration (10 min). At the end of the titration 170 µL of ctDNA was added and the ligand/DNA molar ratios reached values of approximately 1:12. The effect of ligand dilution after the addition of each aliquot did not give an error of more than 5% for the ligand concentration. Nevertheless, the fluorescence emission intensities were corrected due to this dilution. The derivation of the equations for the ligand-macromolecule binding is described in the Supporting Information.

2. DNA melting assay

Synthetic oligodeoxynucleotides with one strand 5'-end-labelled with the fluorophore 6-carboxyfluorescein (6-FAM, F) and the complementary strand 3'-end-labelled with the quencher tetramethylrhodamine (TAMRA, Q) were synthesized and purified by high-performance liquid chromatography as a single peak by biomers.net GmbH (Ulm, Germany). Annealing of each F-oligonucleotide with its complementary Q-oligonucleotide at a final duplex concentration of 0.1 µmol/L in Dulbecco's PBS buffer [137 mM NaCl, 2.7 mM KCl, 8.06 mM Na₂HPO₄, 1.47 mM KH₂PO₄ (pH 7.4), ionic strength 999999] was accomplished in a PTC-100 thermocycler (MJ Research) by first heating to 95 °C for 5 min and then gradually cooling down to 20 °C at a rate of 1 °C/min. Correct annealing was confirmed by monitoring the fluorescence quenching that takes place when F and Q are placed in proximity on formation of a double-stranded structure. The melting reactions were carried out in 96-well plates loaded with the preannealed double-stranded oligonucleotides in a total volume of 20 µL of PBS buffer at a final concentration of 0.1 µmol/L either in the absence or in the presence of each ligand. The ligand was dissolved in DMSO and serially diluted in the same solvent to yield final concentrations from 0.01 to 0.1 µmol/L. The mixtures were incubated for 1 h at 37 °C before the melting assay was started in a 7500 Fast Real-Time PCR System (ABI Prism, Applied Biosystems, Foster City, CA, USA) by increasing the temperature at a rate of 1 °C/min up to 95 °C. The changes in fluorescence at 517 nm in the FAM channel (excitation at 488 nm from argon ion laser line) obtained as a function of the temperature were recorded and the midpoint of the transition (T_m) was calculated. This allowed us to estimate the increases in melting temperatures (ΔT_m) brought about by ligand binding. A series of custom-designed oligonucleotides

were designed to provide at least a single occurrence of all possible 3-base pair long and all possible palindromic 4-base pair long binding sites composed of either A and T or G and C bases. All measurements were carried out at least in duplicate. The raw data recovered from the instrument for each plate consisted of an array of FAM fluorescence values for each of the 96 wells at each temperature. These data were analysed to estimate the increases in melting temperatures (ΔT_m) brought about by ligand binding at the different concentrations analyzed. The numeric analysis was carried out using an in-house developed Visual Basic application running on Microsoft Excel (Microsoft, Redmond, WA, USA).

Acknowledgements

Financial support from the Spanish Ministerio de Economía y Competitividad (project CTQ2011-24715), Instituto de Salud Carlos III (REDinREN, RD12/0021/0014) and University of Alcalá (project CCG2013/EXP-036) and grants for P. B. and R. M. S. are gratefully acknowledged.

Notes and references

^a Departamento de Química Orgánica y Química Inorgánica; Universidad de Alcalá, 28871-Alcalá de Henares, Madrid, Spain.

^b Departamento de Biología de Sistemas; Universidad de Alcalá.

^c Departamento de Química Analítica, Química Física e Ingeniería Química, Universidad de Alcalá.

‡ These authors have contributed equally to this work.

† Electronic Supplementary Information (ESI) available: [¹H and ¹³C NMR data for all new compounds, photophysical and DNA binding experiments and MM and MD protocols]. See DOI: 10.1039/b000000x/

- 1 K. Bhadra and G. S. Kumar, *Med. Res. Rev.*, 2011, **31**, 821.
- 2 M. J. Cho, A. J. Repta, C. C. Cheng, K. Y. Zee-Cheng, T. Higuchi T. and I. H. Pitman, *J. Pharm. Sci.*, 1975, **64**, 1825.
- 3 H. Ihmels, K. Faulhaber, D. Vedaldi, F. Dall'Acqua and G. Viola, *Photochem. Photobiol.*, 2005, **81**, 1107.
- 4 D. Makhey, B. Gatto, C. Yu, A. Liu, L. F. Liu and E. J. LaVoie, *Bioorg. Med. Chem.*, 1996, **4**, 781.
- 5 E. Mateos, V. L. Cebolla, L. Membrado, J. Vela, E. M. Gálvez, M. Matt and F. P. Cossio, *J. Chromatogr. A*, 2007, **1146**, 251.
- 6 H. Ihmels and A. Salbach, *Photochem. Photobiol.*, 2006, **82**, 1572.
- 7 P. Giri and G. S. Kumar, *Mini-Rev. Med. Chem.*, 2010, **10**, 568.
- 8 K. Bhadra and G. S. Kumar, *Biochim. Biophys. Acta*, 2011, **1810**, 485.
- 9 S. Hazra, M. Hossain and G. S. Kumar, *Mol. BioSyst.*, 2013, **9**, 143.
- 10 J. Zhou, D. A. Sayre, Y. Zheng, H. Szmacinski and H. O. Sintim, *Anal. Chem.*, 2014, **86**, 2412.
- 11 S. Hazra, M. Hossain and G. S. Kumar, *J. Incl. Phenom. Macrocycl. Chem.*, 2014, **78**, 311.
- 12 (a) K. Benner, H. Ihmels, S. Kölsch and P. M. Pithan, *Org. Biomol. Chem.*, 2014, **12**, 1725; (b) R. Bortolozzi, H. Ihmels, L. Thomas, M. Tian and G. Viola, *Chem.–Eur. J.*, 2013, **19**, 8736; (c) M. Tian, H. Ihmels and S. Ye, *Org. Biomol. Chem.*, 2012, **10**, 3010; (d) K. Faulhaber, A. Granzhan, H. Ihmels, D. Otto, L. Thomas, S. Wells, *Photochem. Photobiol. Sci.*, 2011, **10**, 1535; (e) H. Ihmels, *Science of Synthesis, Knowledge Updates*, 2011, **1**, 75; (f) A. Granzhan, H.

- Ihmels, G. Viola, *J. Am. Chem. Soc.*, 2007, **129**, 1254; (g) H. Ihmels, *Science of Synthesis*, 2005, **15**, 907.
- 13 (a) C. Norez, C. Jayle, F. Becq and C. Vandebrouck, *Pulm. Pharmacol. Ther.*, 2014, **27**, 38; (b) C. Norez, F. Bilan, A. Kitzis, Y. Mettey and F. Becq, *J. Pharmacol. Exp. Ther.*, 2008, **325**, 89; (c) C. Marivingt-Mounir, C. Norez, R. Dérand, L. Bulteau-Pignoux, D. Nguyen-Huy, B. Viossat, G. Morgant, F. Becq, J.-M. Vierfond, and Y. Mettey, *J. Med. Chem.*, 2004, **47**, 962.
- 14 A. Paul, S. Bhattacharya, *Curr. Sci.*, 2012, **102**, 212.
- 15 H. Ihmels, B. Engels, K. Faulhaber and C. Lennartz, *Chem.–Eur. J.*, 2000, **6**, 2854.
- 16 Strekowski L. *Heterocyclic Polymethine Dyes; Synthesis, Properties and Applications*. In *Top. Heterocycl. Chem.* 2008, 14. Springer GmbH, 2008.
- 17 (a) B. Abarca, R. Custodio, A. M. Cuadro, D. Sucunza, A. Domingo, F. Mendicuti, J. Álvarez-Builla, and J. J. Vaquero, *Org. Lett.*, 2014, **16**, 3464; (b) A. Núñez, B. Abarca, A. M. Cuadro, J. Alvarez-Builla and J. J. Vaquero, *Eur. J. Org. Chem.*, 2011, 1280; (c) A. Núñez, B. Abarca, A. M. Cuadro, J. Alvarez-Builla and J. J. Vaquero, *J. Org. Chem.*, 2009, **74**, 4166; (d) A. Núñez, A. M. Cuadro, J. Alvarez-Builla and J. J. Vaquero, *Org. Lett.*, 2007, **9**, 2977.
- 18 (a) T. Cañeque, A. M. Cuadro, J. Alvarez-Builla and J. J. Vaquero, *Tetrahedron Lett.*, 2009, **50**, 1419; (b) D. García-Cuadrado, A. M. Cuadro, J. Alvarez-Builla, U. Sancho, O. Castaño and J. J. Vaquero, *Org. Lett.*, 2006, **8**, 5955; (c) D. García-Cuadrado, A. M. Cuadro, B. M. Barchin, A. Núñez, T. Cañeque, J. Alvarez-Builla and J. J. Vaquero, *J. Org. Chem.*, 2006, **71**, 7989; (d) D. García, A. M. Cuadro, J. Alvarez-Builla and J. J. Vaquero, *Org. Lett.*, 2004, **6**, 4175.
- 19 (a) T. Cañeque, A. M. Cuadro, J. Alvarez-Builla, J. Pérez-Moreno, K. Clays, O. Castaño, J. L. Andrés and J. J. Vaquero, *Dyes and Pigments*, 2014, **101**, 116; (b) E. Maçõas, G. Marcelo, S. Pinto, T. Cañeque, A. M. Cuadro, J. J. Vaquero and J. M. G. Martinho, *Chem. Commun.*, 2011, **47**, 7374.
- 20 (a) V. Martínez, C. Burgos, J. Alvarez-Builla, G. Fernández, A. Domingo, R. García-Nieto, F. Gago, I. Manzanares, C. Cuevas and J. J. Vaquero, *J. Med. Chem.*, 2004, **47**, 1136; (b) A. Molina, J. J. Vaquero, J. L. García-Navío, J. Alvarez-Builla, B. Pascual-Teresa, F. Gago and M. M. Rodrigo, *J. Org. Chem.*, 1999, **64**, 3907.
- 21 V. García-Hernández, Ph.D. Thesis, University of Alcalá, 2009.
- 22 J. Siro, A. Ramos, J. J. Vaquero, J. Alvarez-Builla and J. L. García-Navío, *Tetrahedron*, 2000, **56**, 2469.
- 23 (a) J. Pastor, J. G. Siro, J. L. García-Navío, J. J. Vaquero, J. Alvarez-Builla, F. Gago, B. de Pascual-Teresa, M. Pastor and M. M. Rodrigo, *J. Org. Chem.*, 1997, **62**, 5476; (b) M. P. Matia, J. L. García-Navío, J. J. Vaquero and J. Alvarez-Builla, *Liebigs Ann. Chem.*, 1992, 777.
- 24 R. Carceller, J. L. García-Navío, M. L. Izquierdo, J. Alvarez-Builla, M. Fajardo, P. Gómez-Sal and F. Gago, *Tetrahedron*, 1994, **50**, 4995.
- 25 I. Santiesteban, J. Siro, J. J. Vaquero, J. L. García-Navío, J. Alvarez-Builla and O. Castaño, *J. Org. Chem.*, 1996, **60**, 5667.
- 26 M. Pereira and V. Thiery, *Org. Lett.*, 2012, **14**, 4754.
- 27 Z. Xu, N. J. Singh, S. K. Kim, D. R. Spring, K. S. Kim and J. Yoon, *Chem. Eur. J.*, 2011, **17**, 1163.
- 28 J. Mendiola, J. A. Rincón, C. Mateos, J. F. Soriano, O. de Frutos, J. K. Niemeier and E. M. Davis, *Org. Process Res. Dev.*, 2009, **13**, 263.
- 29 F. Mendicuti and W. L. Mattice, *Polym. Bull.*, 1989, **22**, 557.
- 30 (a) H. Ihmels, K. Faulhaber, K. Wissel, G. Bringmann, K. Messer, G. Viola and D. Vedaldi, *Eur. J. Org. Chem.*, 2001, 1157; (b) M. Torimura, S. Kurata, K. Yamada, T. Yokomaku, Y. Kamagata, T. Kanagawa and R. Kurane, *Anal. Sci.*, 2001, **17**, 155; (c) C. A. M. Seidel, A. Schulz and M. H. M. Sauer, *J. Phys. Chem.*, 1996, **100**, 5541.
- 31 (a) M. Ardhammar, B. Nordén and T. Kurucsev, In *Circular Dichroism: Principles and Applications*, Berova, N.; Nakanishi, K.; Woody, R. W.; Editors, Eds. Wiley-VCH: Weinheim, 2000; p. 741; (b) W. C. Johnson, In *Circular Dichroism: Principles and Applications*, Berova, N.; Nakanishi, K.; Woody, R. W.; Editors, Eds. Wiley-VCH: Weinheim, 2000; p. 703.
- 32 (a) M. N. Dehkordi, A.-K. Bordbar, P. Lincoln and V. Mirkhani, *Spectrochim. Acta Mol. Biomol. Spectros.*, 2012, **90**, 50; (b) K. Triantafillidi, K. Karidi, O. Novakova, J. Malina and A. Garoufis, *Dalton Trans.*, 2011, **40**, 472; (c) J. Kyrp, I. Kejnovska, D. Renciuik and M. Vorlickova, *Nucleic Acids Res.*, 2009, **37**, 1713; (d) K. Karidi, A. Garoufis, N. Hadjiliadis and J. Reedijk, *Dalton Transactions*, 2005, 728.
- 33 (a) S. Basili, A. Bergen, F. Dall'Acqua, A. Faccio, A. Granzhan, H. Ihmels, S. Moro and G. Viola, *Biochemistry*, 2007, **46**, 12721; (b) B. Nordén and T. Kurucsev, *J. Mol. Recognit.*, 1994, **7**, 141.
- 34 D. V. O'Connor, W. R. Ware and J. C. Andre, *J. Phys. Chem.*, 1979, **83**, 1333.
- 35 *Sybyl-X 2.0, Tripos International.*, 1699 South Hanley Rd., St. Louis, Missouri, 63144, USA.
- 36 M. Clark, R. D. Cramer III and O. N. Van, *J. Comput. Chem.*, 1989, **10**, 982.
- 37 M. J. Frisch, H. B. Schlegel, G. E. Scuseria, M. A. Robb, J. R. Cheeseman, G. Scalmani, V. Barone, B. Mennucci, G. A. Petersson, H. Nakatsuji, M. Caricato, X. Li, H. P. Hratchian, A. F. Izmaylov, J. Bloino, G. Zheng, J. L. Sonnenberg, M. Hada, M. Ehara, K. Toyota, R. Fukuda, J. Hasegawa, M. Ishida, T. Nakajima, Y. Honda, O. Kitao, H. Nakai, T. Vreven, J. A. Montgomery J, J. E. Peralta, F. Ogliaro, M. Bearpark, J. J. Heyd, E. Brothers, K. N. Kudin, V. N. Staroverov, R. Kobayashi, J. Normand, K. Raghavachari, A. Rendell, J. C. Burant, S. S. Iyengar, J. Tomasi, M. Cossi, N. Rega, J. M. Millam, M. Klene, J. E. Knox, J. B. Cross, V. Bakken, C. Adamo, J. Jaramillo, R. Gomperts, R. E. Stratmann, O. Yazyev, A. J. Austin, R. Cammi, C. Pomelli, J. W. Ochterski, R. L. Martin, K. Morokuma, V. G. Zakrzewski, G. A. Voth, P. Salvador, J. J. Dannenberg, S. Dapprich, A. D. Daniels, Ö. Farkas, J. B. Foresman, J. V. Ortiz, J. Cioslowski and D. J. Fox, Gaussian 09, Revision A.1. ed. Wallingford, CT, USA: Gaussian, Inc.; 2009.
- 38 M. Blanco, *J. Comput. Chem.*, 1991, **12**, 237.
- 39 Y. Brunel, H. Faucher, D. Gagnaire and A. Rassat, *Tetrahedron*, 1975, **31**, 1075.
- 40 A. W. McConnaughie and T. C. Jenkins, *J. Med. Chem.*, 1995, **38**, 3488.